Appl. Phys. B 61, 207–211 (1995)

Applied Physics B Lasers and Optics

Characterization of the KNSBN:Cu crystal with two-wave coupling at visible and infrared wavelengths

H. Zhang[1], B. Guo[2], H. Jiang[1], Y. Shih[1], L. Yan[2]

[1] Department of Physics, University of Maryland, Baltimore, MD 21228, USA
(Fax: +1-410/455-1072.)
[2] Department of Electrical Engineering, University of Maryland, Baltimore, MD 21228, USA

Received: 15 August 1994/Accepted: 5 October 1994

Abstract. We have optically characterized the newly-developed photorefractive crystal KNSBN:Cu by two-wave coupling at visible and near-infrared wavelengths. The effective electrooptic coefficients $\xi(k_g)r_{13}$ and $\xi(k_g)r_{33}$, the effective charge carrier density N_{eff}, the dark conductivity σ_d, the product of mobility and electron-trap recombination time $\mu\tau_R$, the formation and decay rate of index grating and the absorption coefficient α of the crystal were determined from visible to near-infrared wavelengths. Their wavelength dependences were also studied. It is interesting to notice that the KNSBN:Cu crystal has a very large N_{eff} and large gain coefficient Γ for ordinary ray (o-ray) in the visible region, and the photorefractive properties of the crystal are very different in the visible and near-infrared spectral regions.

PACS: 42.70.Gz; 42.30.Va; 42.40.Kw; 42.65

Photorefractive crystals have been used to demonstrate a wide range of nonlinear optical applications, such as optical phase conjugation, real-time information processing, holographic optical storage, coherent light amplification, etc [1–4]. To reach the final stage of these applications, the development and characterization of new photorefractive materials are of great significance.

Over the years, many kinds of photorefractive materials, such as $LiNbO_3$, BSO, $BaTiO_3$, and SBN have been studied [15, 16]. Recently, a new photorefractive crystal BSKNN ($Ba_{2-x}Sr_xK_{1-y}Na_yNb_5O_{15}$) based on SBN gave rise to great interest [7, 8]. In [8], the crystal is called KNSBN with the chemical formula as $(K_{0.5}Na_{0.5})_{0.2}(Sr_{0.75}Ba_{0.25})_{0.9}Nb_2O_6$.] It not only showed good properties in photorefractive applications [9], but was also easy to grow, develop and pole.

In this paper, we present the results of characterization of KNSBN:Cu by the method of two-wave coupling. KNSBN:Cu is one of the crystals in the KNSBN family. The crystal was grown by Coretech Crystal Co., Shandong, China. The chemical formula of the crystal characterized is $(K_{0.5}Na_{0.5})_{0.2}(Sr_{0.75}Ba_{0.25})_{0.9}Nb_2O_6$ with 0.1 wt% of Cu. The size of the crystal is $5 \times 5 \times 5$ mm^3 with a dielectric constant $\varepsilon_{33} = 260$, and the extra-ordinary and ordinary refractive indexes $n_e = 2.28$ and $n_o = 2.31$ at 632.8 nm, respectively.

Our experiments consisted of two parts. The first part is the measurements of steady-state parameters. We measured the effective electrooptic coefficient, the effective charge-carrier density, and the absorption coefficient. In the second part, we measured the dynamic parameters of the KNSBN:Cu crystal: the index-grating formation and decay rates, the dark conductivity, and the product of mobility and electron-trap recombination time. All these parameters were measured in the visible and near-infrared spectral region.

1 Characterization of the steady state photorefractive parameters

1.1 Theoretical bases

The electrooptic coefficients and the effective charge-carrier density N_{eff} of KNSBN:Cu can be determined by measuring the gain coefficient Γ in two-wave coupling. Figure 1 depicts the geometry of the two-wave coupling experiment. The pump and signal beams are incident symmetrically into the crystal, and the **k** vector of the photorefractive grating is along the C-axis of the crystal.

According to two-wave coupling theory [10], the intensities of the signal and pump beams are related by

$$I_s/I_{s0} = I_{p0}/I_p e^{\Gamma L}, \tag{1}$$

where I_{s0} and I_s are the intensities of the transmitted signal beam without and with pump beam, respectively, I_{p0} and I_p are the intensities of the transmitted pump beam without and with signal beam, respectively, L is the

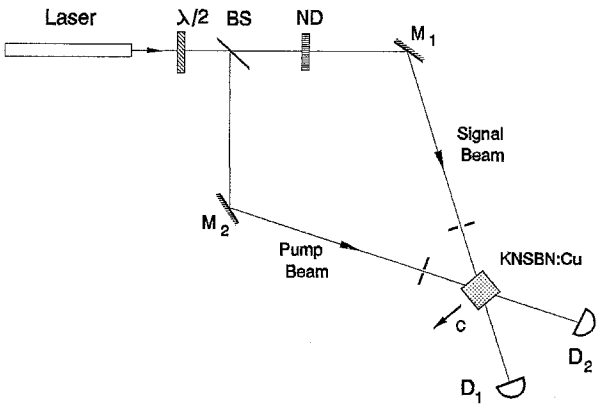

Fig. 1. Experimental setup for two-wave coupling

effective interaction length, and Γ is the coupling strength, and is given by [11, 12]:

$$\Gamma = \frac{\omega n^3}{c} \frac{E_{SC} r_{eff}}{m \cos\theta_i}, \tag{2}$$

where ω is the optical frequency, c is the speed of light, n is the refractive index, $2\theta_i$ is the internal cross angle, r_{eff} is the effective electrooptic coefficient, and m is modulation depth. E_{SC} is the photoinduced space-charge electric field and is given by [12]:

$$E_{SC} = m\left(\frac{k_B T}{e}\right) \frac{k_g}{1 + \left(\frac{k_g}{k_0}\right)^2} \xi(k_g) \mathbf{e}_1 \mathbf{e}_2, \tag{3}$$

where $\xi(k_g)$ is the electron-hole competition factor [12], $\mathbf{e}_1$ and $\mathbf{e}_2$ are the unit vectors of the electric field of the pump and signal beams,

$$k_g = 2\pi/\Lambda_g = 4\pi \sin\theta/\lambda, \tag{4}$$

where Λ_g is the spacing of the index grating, λ is the wavelength of light in vaccum, 2θ is the external cross angle of signal and pump beams, and

$$k_0 = \sqrt{\frac{e^2 N_{eff}}{\varepsilon\varepsilon_0 k_B T}} \tag{5}$$

is the inverse Debye-screening length. Combining (1) and (2), we have

$$\Gamma = \frac{A \sin\theta}{1 + \frac{\sin^2\theta}{B^2}} \frac{\mathbf{e}_1 \mathbf{e}_2}{\cos\theta_i}, \tag{6}$$

where

$$A = \xi(k_g) r_{eff} \frac{8\pi^2 n^3 k_B T}{e\lambda^2}, \tag{7}$$

$$B = \frac{\lambda k_0}{4\pi} = \frac{e\lambda}{4\pi} \sqrt{\frac{N_{eff}}{\varepsilon\varepsilon_0 k_B T}}. \tag{8}$$

A and B can be derived by best fitting of the experimental results of the gain coefficient Γ versus external cross angle 2θ. One can then determine N_{eff} from B, and $\xi(k_g) r_{eff}$ from A. The effective electrooptic coefficient r_{eff} is dependent on the electrooptic coefficients of the crystal, the geometry, and the polarization of the two coupling beams. In the configuration of our experiment, when the signal and pump beams are ordinary waves [13, 14],

$$\mathbf{e}_1 \mathbf{e}_2 = 1, \tag{9a}$$

$$r_{eff} = r_{13}, \tag{9b}$$

and, when the beams are extraordinary waves [13, 14],

$$\mathbf{e}_1 \mathbf{e}_2 = \cos 2\theta_i, \tag{10a}$$

$$r_{eff} = r_{33} \cos^2\theta_i - r_{13} \sin^2\theta_i + \frac{\Delta n}{n_e}(r_{33} + r_{13}) \sin^2 2\theta_i$$

$$\approx r_{33} \text{ when } \theta_i \text{ is very small}, \tag{10b}$$

where $\Delta n = n_e - n_o \ll n$, and $n = n_e n_o (n_e^2 \sin^2\theta_i + n_o^2 \cos^2\theta_i)^{-1/2}$.

Thus, keeping the same cross angles and measuring the coupling gain coefficient Γ for the o-ray and e-ray, respectively, we have,

$$\frac{\Gamma_o}{\Gamma_e} = \frac{r_{13}}{r_{33}}. \tag{11}$$

1.2 Experiments and discussions

The experiment was performed in both the visible and near-infrared spectral region. In the visible region, we used different wavelengths of an argon-ion laser: 514.5, 496.5, 488.0, and 476.5 nm. In the near-infrared region we used a Ti: Sapphire laser. The wavelengths of 706.1, 750.0, and 810.0 nm were used.

In the experiment at visible wavelengths, we chose the pump and signal beams to be polarized as ordinary waves, because when using extraordinary rays, the gain coefficient Γ can not be measured accurately due to the strong fanning effect in the crystal. With the choice of o-ray polarization, according to (6) and (9)

$$\Gamma = \frac{A \sin\theta}{1 + \frac{\sin^2\theta}{B^2}} \frac{1}{\cos\theta_i}. \tag{12}$$

Figure 2 shows the measured gain coefficient Γ as a function of the external cross angle of pump and signal beams at 514.5, 496.5, 488.0, and 476.5 nm. The solid curves are best fits of equation (12) and yield values of parameters A and B. From A and B, we derived $\xi(k_g) r_{13}$ and N_{eff}.

It is interesting to note that the KNSBN:Cu has a large gain coefficient Γ for o-rays in the visible region. This is because it has a very large N_{eff} at these wavelengths. According to (6–8), around the cross angle of maximum gain, the gain coefficient Γ is proportional to $r_{eff} N_{eff}^{1/2}$ because the two-wave coupling-gain coefficient Γ for the o-ray is considerably large although the electrooptic coefficient $\xi(k_g) r_{13}$ is relatively small. The very large N_{eff} (and therefore, B) makes the maxium gain coefficient Γ appearing at a very large cross angle 2θ. This is different from other photorefractive materials, such as SBN, where the gain for the o-ray is much smaller compared to KNSBN:Cu, and Γ appears at a much smaller cross angle, usually less than 20° [15, 16].

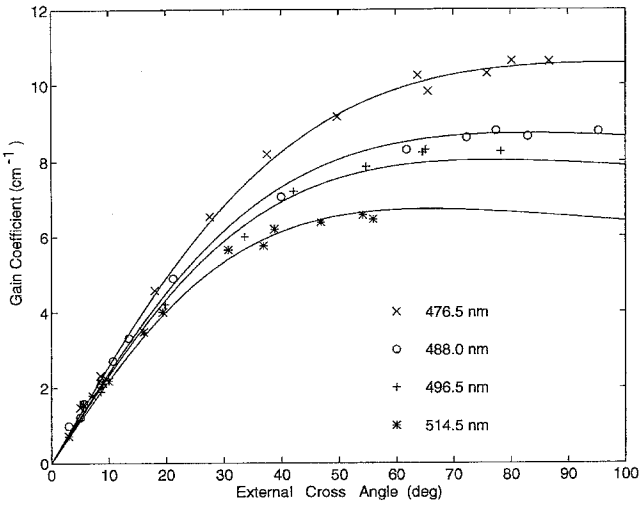

Fig. 2. Gain coefficient Γ vs external cross angle 2θ at visible wavelengths

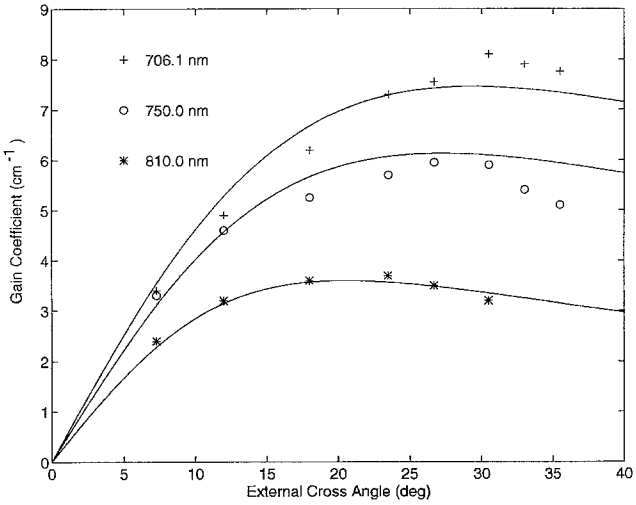

Fig. 3. Gain coefficient Γ vs external cross angle 2θ at near-infrared wavelengths

The same measurements were performed in the near-infrared, except that extraordinary rays were chosen as pump and signal beams, and

$$\Gamma = \frac{A \sin\theta}{1 + \dfrac{\sin^2\theta}{B^2}} \frac{\cos 2\theta_i}{\cos\theta_i}. \tag{13}$$

Figure 3 shows the experimental results and the fitted curves for Γ versus cross angle 2θ according to (13) at 706.1, 750.0, and 810.0 nm. The parameters $\xi(k_g)r_{33}$ and N_{eff} were derived from the fitted A and B. Table 1 summerizes the experimental results of the steady-state parameters of the KNSBN:Cu crystal.

From the values of $\xi(k_g)r_{13}$, $\xi(k_g)r_{33}$, and N_{eff}, we found that within the visible and near-infrared, respectively, the product of electron-hole competition factor and the effective electrooptic coefficient $\xi(k_g)r_{13}$ and $\xi(k_g)r_{33}$ show little wavelength dependence. Their average values are

$$\overline{\xi(k_g)r_{13}} = 27.3\,\text{pm/V}, \tag{14}$$

$$\overline{\xi(k_g)r_{33}} = 115.0\,\text{pm/V}, \tag{15}$$

On the other hand, the effective charge-carrier density N_{eff} is strongly dependent on wavelength. We also measured the absorption coefficient α at visible to near-infrared wavelengths. Figure 4 gives the experimental results of α and N_{eff} at visible to near-infrared wavelengths. It is noticed that both N_{eff} and α decrease drastically as the wavelength increases. N_{eff} decreases by more than 30 times when the wavelength increases from 476.5 to 706.1 nm, while the absorption coefficient α at 476.5 nm is also more than 30 times larger than that at 706.1 nm. From Fig. 4, one can see a clear correlation between N_{eff} and α.

In the near-infrared at $\lambda = 706.1$ nm, we also measured the two-wave coupling gain coefficient Γ using both e-rays and o-rays at an external cross angle $2\theta = 7.6°$. We obtained $\Gamma_e = 2.96\ \text{cm}^{-1}$ and $\Gamma_o = 0.59\ \text{cm}^{-1}$. Since $\xi(k_g)$ is independent on the polarization, and, in our experiment

Table 1. Steady-state photorefractive parameters

λ [nm]	Γ_{max} [cm^{-1}]	N_{eff} [10^{16} cm^{-3}]	α [cm^{-1}]	$\xi(k_g)r_{13}$ [pm/V]	$\xi(k_g)r_{33}$ [pm/V]
476.5	10.63	11.7	4.14	27.4	
488.0	8.80	9.0	3.16	27.4	
496.5	8.00	7.9	2.47	27.0	
514.5	6.57	5.8	1.50	27.4	
706.1	8.10	0.46	0.13		119
750.0	5.95	0.26			119
810.0	3.70	0.13			107

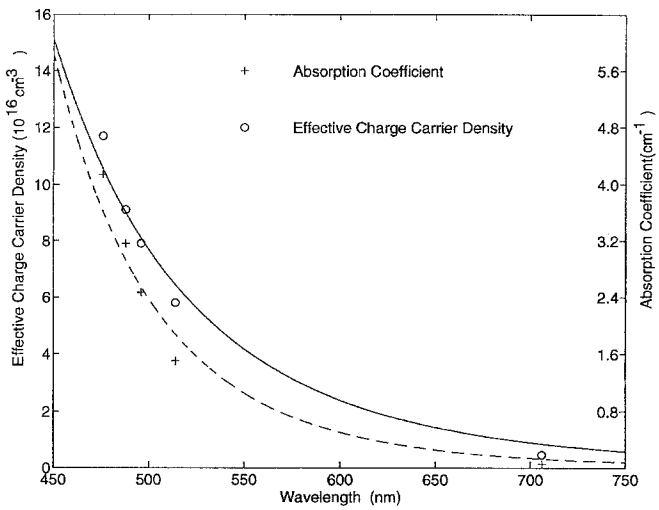

Fig. 4. Wavelength dependence of effective charge-carrier density N_{eff} and absorption coefficient α

with e-rays, the external cross angle 2θ corresponding to the maximum gain was about 20–30°, and $r_{eff} \approx r_{33}$ with an error less than 1.6%, we used (10) to derive $\xi(k_g)r_{13}$ in the near-infrared region with $\xi(k_g)r_{33} = 115.0$ pm/V from the previous e-ray experiment, and obtained $\xi(k_g)r_{13} = 24$ pm/V, which is a little smaller than the

result given by (14). Because the electrooptic coefficient r_{13} is independent of wavelength, the difference between the values of $\xi(k_g)r_{13}$ derived in visible and near infrared is due to the factor $\xi(k_g)$. This indicates that the electron-hole competition factor is a little smaller in the near-infrared region.

2 Dynamic photorefractive parameters

2.1 Measurements of σ_d and $\mu\tau_R$

We determined the dark conductivity σ_d and the product of mobility and recombination time $\mu\tau_R$ by measuring the decay rate as a function of the intensity of the erasing beam. When there is no externally applied electric field and, in the limit that the grating spacing is much larger than the diffusion length $l_d = (\mu\tau_R k_B T/e)^{1/2}$ [6, 17]. the photorefractive index decay rate τ^{-1} can be written as [6, 17]:

$$\tau^{-1} = (\sigma_d + \frac{e}{hc}\alpha\mu\tau_R\lambda I)/\varepsilon\varepsilon_0, \tag{16}$$

where σ_d, $\mu\tau_R$, l_d, and $d\tau^{-1}/dI$ can be determined from the experimental plot of τ^{-1} versus intensity I.

To determine the light-induced decay rate, a refractive-index grating was created by illuminating the KNSBN:Cu crystal with two writing beams. (They are called pump and signal beams in the two-wave coupling scheme). We set the external cross angles to be 53.3° for 488.0 and 514.5 nm, and 78.8° for 702 nm so that the index-grating spacings were approximately the same. After the steady state was achieved (it took several seconds at visible wavelengths and several minutes at 706.1 nm), one writing beam (signal beam) was blocked, and an erasing beam was incident along the direction of the pump beam. The intensity of the Bragg-reflected erasing beam in the direction of the transmitted signal beam was recorded. Figure 5 shows the measured exponential decay rate τ^{-1} versus the erasing beam intensity I. Table 2 summerizes the deduced results. We see that $l_d \ll \Lambda_g/2\pi$ in the three cases, consistent with the assumption for using (16).

The decay rate at 1W/cm^2 for 514.5 and 488.0 nm are of the same order of magnitude, 1.0 s^{-1}, while for 702.0 nm the decay rate 3.37×10^{-3} s^{-1} is much smaller than that in the visible region. The dark conductivities σ_d at 514.5 and 488.0 nm are about the same, while they are much smaller at 702.0 nm. The value of $\mu\tau_R$ at 702.0 nm is also 20 times smaller than that at the visible wavelengths. This indicates that the photorefractive charge carriers for visible and near-infrared wavelengths are due to the excitation (ionization) of electrons from different energy levels of the impurity in KNSBN:Cu. Thus, KNSBN:Cu shows much different photorefractive properties at visible and near-infrared wavelengths, which may lead to different applications by using different wavelengths. For example, at visible wavelengths KNSBN:Cu can be applied to phase conjugation [8, 9], while a near-infrared wavelengths, it is a very good candidate for optical holographic storage.

2.2 Measurement of index-grating-formation rate

The index grating is created by the interference of two writing beams. The interfering intensity distribution is given by:

$$I(z) = I_0[1 + m\cos(k_g z)]$$
$$= I_0 + mI_0\cos(k_g z), \tag{17}$$

where

$$m = \frac{2\sqrt{I_1 I_2}}{I_1 + I_2} \tag{18}$$

is the modulation depth, I_1, I_2 are the intensities of the two writing beams, and

$$I_0 = I_1 + I_2$$

is the total intensity.

Unlike the decay rate, the formation rate is not only a function of the total intensity of the two writing beams,

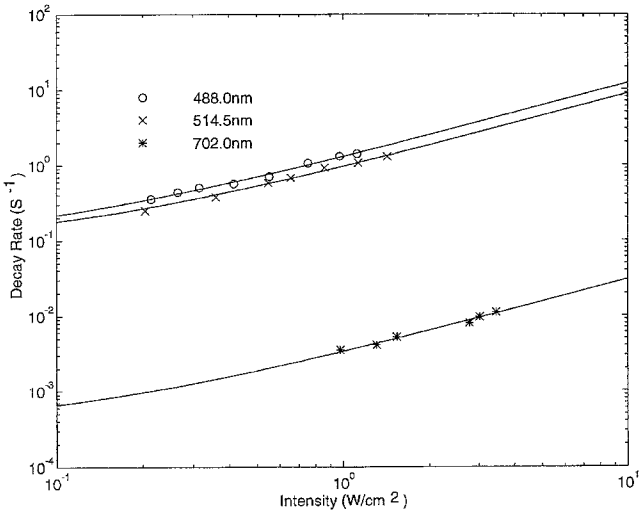

Fig. 5. Index-grating decay rate vs erasing intensity at visible and near-infrared wavelengths

Table 2. Dynamic photorefractive parameters

λ [nm]	α [cm^{-1}]	σ_d [(Ωcm)$^{-1}$]	$\mu\tau_R$ [cm^2/V]	l_d [nm]	Λ_g [nm]	τ^{-a} [s^{-1}]
488.0	3.16	2.08×10^{-11}	3.23×10^{-11}	9.16	545.8	1.30
514.0	1.50	2.22×10^{-11}	2.24×10^{-11}	7.63	575.8	0.96
702.0	0.13	8.28×10^{-14}	9.44×10^{-14}	0.50	575.5	3.37×10^{-3}

[a] Value at 1W/cm^2

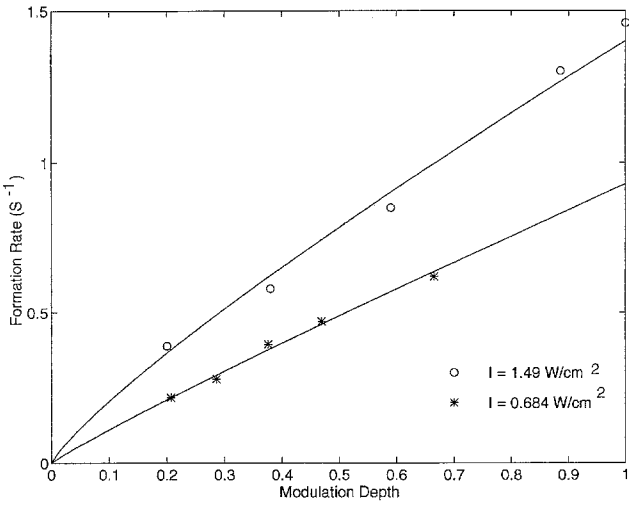

Fig. 6. Relationship between index-grating-formation rate and the modulation depth m

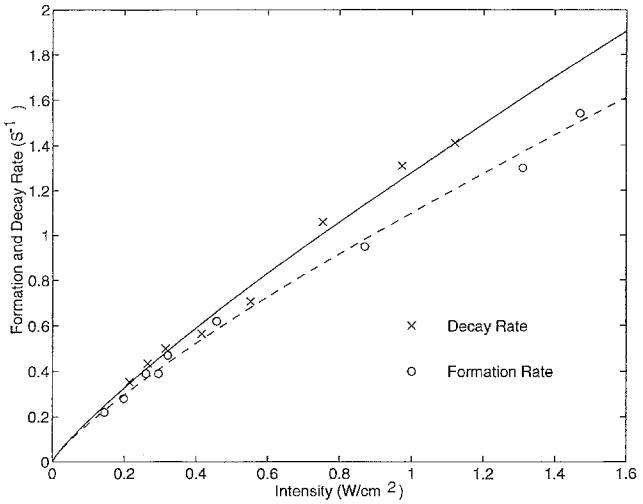

Fig. 7. Comparision of formation rate and decay rate of the index grating

but also varies with their modulation depth m. In (17), only the modulation of the total intensity mI_0 contributes to the formation of the index grating, while the dc component does not.

We measured the formation rate of the index grating in KNSBN:Cu at the wavelength of 488.0 nm. With the total intensity of the incident beams kept constant, we measured the formation rate with different modulation depths m at 488.0 nm. Figure 6 shows the experimental results with the total intensity I_0 kept as 0.684 W/cm^2 and 1.49 W/cm^2, respectively. It is noticed that with the total intensity kept constant, the formation rate is a sublinear function of the modulation depth m.

In Fig. 7, we replot the experimental results in Fig. 6 with the formation rate as the ordinate, and mI_0, the product of total intensity I_0 and modulation depth m, as the abscissa. For comparison with the decay rate at the same wavelength, the experimental results of the decay rate versus intensity at 488.0 nm are also reploted in Fig. 7, with the erasing intensity as abscissa and the decay rate as ordinate. We find that the formation rate and the decay rate are close to each other when the value of mI_0 equals the erasing intensity. At 1 W/cm^2, the formation rate and the decay rate at 488.0 nm are about 1.2 s^{-1}.

3 Conclusion

In summary, we have thoroughly characterized the photorefractive properties of the KNSBN:Cu crystal. The product of the electron-hole competition factor and the electrooptic coefficient $\xi(k_g)r_{13}$ were measured to be 27.3 pm/V and $\xi(k_g)r_{33} = 115$ pm/V, respectively. The KNSBN:Cu crystal has a very large N_{eff} and a large gain coefficient Γ for o-rays at visible wavelengths (10.7 cm^{-1} at 476.5 nm). Because the electrooptic coefficient r_{33} is much larger than r_{13} for KNSBN:Cu, the KNSBN:Cu crystal is expected to have a very much larger gain for e-rays in the visible region. The effective charge-carrier density N_{eff} is strongly dependent on wavelength, and changes from 0.46×10^{16} to 11.7×10^{16} cm^{-3} from 706 to 476 nm. The absorption coefficient α of the crystal is between 0.13–4.14 cm^{-1} from 706 to 476 nm. There is a clear correlation between N_{eff} and α. KNSBN:Cu also shows a large difference in dark conductivity σ_d, the product of mobility and electron-trap recombination time $\mu\tau_R$, and the decay rate τ^{-1} at visible and near-infrared wavelengths. At 488.0 nm $\sigma_d = 2.08 \times 10^{-11}$ $(\Omega\text{cm})^{-1}$, $\mu\tau_R = 3.23 \times 10^{-11}$ cm^2/V, and $\tau^{-1} = 1.2$ s^{-1} at 1W/cm^2, while at 702 nm, $\sigma_d = 0.828 \times 10^{-13}$ $(\Omega\text{cm})^{-1}$, $\mu\tau_R = 0.944 \times 10^{-13}$ cm^2/V, and $\tau^{-1} = 3.7 \times 10^{-3}$ s^{-1} at 1W/cm^2. At the visible and near-infrared wavelengths, the photorefractive properties of the crystal are quite different. This may lead to different applications of KNSBN:Cu by using different wavelengths. The nonlinear optical applications of KNSBN:Cu at visible and near-infrared wave-lengths are promising.

References

1. J. Feinberg, R.W. Hellwarth: Opt. Lett. **5**, 519 (1980)
2. J.R. Huignard, A. Marrakchi: Opt. Commun. **38**, 249 (1981)
3. J. Feinberg: Opt. Lett. **5**, 330 (1980)
4. A.E. Chiou, P. Yeh: Opt. Lett. **11**, 306 (1986)
5. R.R. Neurgaonkar, W.K. Cory: J. Opt. Soc. Am. B **3**, 274 (1986)
6. P. Gunter: Phys. Rep. **93**, 199 (1982)
7. R.R. Neurgaonkov, W.K. Cory, J.R. Oliner, M.D. Ewbank, W.F. Hall: Opt. Eng. **26**, 392 (1987)
8. J. Xu, S. Liu, Y. Wu, G. Zhang, Y Son, H. Chen: Opt. Commun. **80**, 239 (1991)
9. J. Xu, Y. Wu, S. Liu, G. Zhang, D. Sun, Y. Song, H. Chen: Opt. Lett. **16**, 1255 (1991)
10. K. MacDonald, J. Feinberg: J. Opt. Soc. Am. **73**, 548 (1983)
11. P. Yeh: J. Opt. Soc. Am. B **2**, 1924 (1985)
12. F.P. Strohkendl, J.M.C. Jonathan, R.W. Hellwarth: Opt. Lett. **11**, 312 (1986)
13. J. Feinberg, D. Heiman, A. Tanguay, R. Hellwarth: J. Appl. Phys. **51**, 1297 (1980)
14. J. Feinberg, R.W. Hellwarth: Opt. Lett. **5**, 519 (1980); **6**, 257 (E) (1981)
15. M.D. Ewbank, R.R. Neurgaonkar, W.K. Cory, J. Feinberg: J. Appl. Phys. **62**, 15 (1987)
16. G.L. Wood, W.W. Clark, III, M.J. Miller: IEEE J. QE-**23**, 2126 (1987)
17. M.B. Klein: Opt. Lett. **9**, 350 (1984)